Suppressing circ_0008494 inhibits HSC s activation by regulating the miR-185-3p/ Col1a1 axis

Binbin Li
Naval Medical University
Jiaming Zhou (zhoujiaming@ntu.edu.cn)
Naval Medical University
Yuanyuan Luo
Tongji University Dongfang Hospital
kegong Tao
Tongji University Dongfang Hospital
Lifen Zhang
Naval Medical University
Yong Lin
Naval Medical University
Xing Zeng
Tongji University Dongfang Hospital
Hongyu Yu
Naval Medical University

Research Article

Keywords: circ_0008494, hepatic fibrosis, hepatic stellate cells, miR-185-3p, Col1a1, sponge, FGF5, BRD4, treatment target, activation

Posted Date: March 29th, 2022

DOI: https://doi.org/10.21203/rs.3.rs-1424258/v1

Abstract

Background

Because of its viral nature and the increasingly metabolic chronic liver diseases, hepatic fibrosis (HF) has become a major challenge to global health. However, there are still no approved effective therapies for HF. Circular RNAs (circRNAs) have emerged as new potential targets of liver diseases. Thus, this research aims to clarify the role of circ_0008494 in liver fibrosis and reveal its mechanism.

Methods

circRNA profiles were screened by RNA sequencing and the location of circ_0008494 was confirmed by fluorescence in situ hybridization assay in human liver fibrosis tissues. Bioinformatics analysis was used for result prediction and dual luciferase reporter, together with AGO-RIP and biotin-coupled miRNA capture assays, were used to determine miR-185-3p/collagen type I alpha 1 chain (Col1a1) as the target of circ_0008494. A stable circ_0008494-interfering cell line of the hepatic stellate cells (HSCs) was constructed and used to determine the regulatory mechanism of circ_0008494/ miR-185-3p/ Col1a1 axis.

Results

Hsa_circ_0008494 was significantly over-expressed and uniquely located at the cytoplasm of HSCs in human HF tissues. Together, dual luciferase reporter, AGO-RIP and biotin-coupled miRNA capture assays validated that circ_0008494 acted as a sponge of miR-185-3p. Rescue assays demonstrated suppressing circ_0008494 could inhibit HSCs' activation, proliferation, migration and promote their apoptosis through miR-185-3p. In particular, the fibrosis indicator, Col1a1, was predicted as the direct target of miR-185-3p and the suppression of circ_0008494 inhibited the expression of Col1a1 by releasing miR-185-3p.

Conclusions

Knocking down circ_0008494 ameliorated fibrosis through the miR-185-3p/Col1a1 axis. circ_0008494 could be a promising treatment target for hepatic fibrosis.

Introduction

Hepatic fibrosis (HF) is the central pathological process of various chronic liver diseases, including alcoholism, chronic viral hepatitis, autoimmune diseases and fatty liver[1]. While the prevalence of viral hepatitis has traditionally been the main cause of the disease, the rapid increase of metabolic liver diseases (e.g., NAFLD / NASH) in recent years has become a new unavoidable risk factor for liver fibrosis[2]. Without appropriate intervention, HF can progress to liver cirrhosis, or even the lethal cancer hepatocellular carcinoma (HCC), which has been deemed a major challenge to global health[3]. However,

as of now, there is no effective treatment for HF. Hepatic stellate cells (HSCs) play a key role in the initiation of liver fibrosis. When responding to injury or inflammatory stimuli, HSCs are activated to produce excessive extracellular matrix (ECM), including mainly collagen I and collagen III[4, 5]. Thus, the strategies to inhibit the HSCs activation and collagens deposition are critical to the prevention and treatment of HF.

In recent years, studies have revealed that non-coding RNAs cooperate in liver fibrosis and are correlated with the severity of liver fibrosis. These include microRNAs (miRNAs), long non-coding RNAs (lncRNAs) and circRNAs[6–9]. circRNA is a novel type of non-coding RNA characterized by a covalent closed-loop structure without 5' to 3' ends or a poly-A tail. It has the quality of high stability, conservation and is specifically expressed in different organs and tissues[10, 11]. circRNAs can be sorted into three types: ecircRNAs (exonic circRNAs), ciRNAs (intronic circRNAs) and elciRNAs (exon-intron circRNAs). Out of the three, elciRNAs/ciRNAs are reported to be mainly involved in gene transcription and are usually located in the cell nucleus[12]. Conversely, most ecircRNAs are commonly found in the cell cytoplasm. They contain miRNA response elements (MREs) and act as competitive endogenous RNAs (ceRNAs) by sponging miRNAs[13, 14].

In recent years, it has been agreed upon that circRNAs play an important regulatory role in a variety of liver diseases. They are said to present as a diagnostic marker and serve as a potential therapeutic target in non-alcoholic fatty liver disease, nonalcoholic steatohepatitis, hepatitis and hepatocellular carcinoma[2, 15–21]. However, the exact mechanism of circRNA and its ceRNA networks in liver fibrosis remain unclear. Therefore, there is a need for further research to illuminate the role of circRNAs in liver fibrosis and HSCs activation and explored its clinical significance. In this research, it is first discovered that circ_0008494 served as a new regulator in liver fibrosis. circ_0008494 regulated the activation of HSCs by sponging miR-185-3p and particularly targeting collagen type I alpha 1 chain (Col1a1), thus it may serve as a promising therapeutic target of hepatic fibrosis.

Materials And Methods

Patient samples

All liver tissue samples in this study were collected from the Second Affiliated Hospital of Naval Medical University, Shanghai, China. Proper amounts of samples were collected for formalin fixation, paraffin embedding and HE staining. All the samples were identified by two professional pathologists (**supplementary Fig. 1**). The staging of liver fibrosis was determined based on the Metavir semi-quantitative evaluation system. 6 human liver fibrosis tissues were used for transcriptome sequencing (RNA-seq). In addition, 22 hepatic fibrosis tissues were used for further detection of the expression of hsa_circ_0008494. All tissue samples were stored in liquid nitrogen until use. The research was approved by the Research Ethics Committee of Second Affiliated Hospital of Naval Medical University, Shanghai, China. Informed written consent was obtained from each sampled patient.

Cell culture

The human HSC cell line LX-2 was cultured in Dulbecco's modified Eagle's medium, supplemented with 100 U/mL penicillin, 100 mg/mL streptomycin (Beyotime, Shanghai, China) and 10% fetal bovine serum (Gibco, New York, NY, USA) at 37 ºC in an atmosphere of 5% CO_2. Recombinant human TGF-β1 (PeproTech, NJ, USA) was used to activate LX-2 cells.

Animals

Male Balb/c mice（6~8 weeks old) were purchased from the Chinese Academy of Sciences (Shanghai, China). The mice were fed in SPF facilities and the methods were approved by the Research Ethics Committee of Second Affiliated Hospital of Naval Medical University, Shanghai, China. For the dimethyl nitrosamine (DMN)-induced hepatic fibrosis model, 20 mice (body weight of 20 ± 3g) received 0.08％DMN on every Monday, Tuesday and Wednesday morning for three consecutive weeks. The control group was given saline injections. The DMN-induced hepatic fibrosis animal model was identified and evaluated by a senior pathologist.

Fluorescence in situ hybridization

The expression level of hsa_circ_0008494 in liver tissues was evaluated by fluorescence in situ hybridization (FISH) assay using a specific Cy3-labeled-circ_0008494 probe (circ103134, Ruibo Bio, Guangzhou, China) and Fluorescent in Situ Hybridization Kit (C10910，Ruibo Bio, Guangzhou, China). After prehybridization, tissue sections were hybridized in hybridization buffer with Cy3-labeled-circ_0008494 probe overnight at 37ºC according to the manufacturer's procedures. After cleansing with hybrid wash buffer I, II, III and counterstaining by 4',6-Diamidino-2-phenylindole (DAPI), the images were acquired under the fluorescent microscope (Zeiss, Thornwood, USA).

RNA-seq array

Six liver fibrosis tissues were used for RNA sequencing (RNA-seq) detection. The clinical information of patients is presented in **Table1**. All RNA samples for RNA-seq were of high-quality with a 28S/18S ratio ≥ 1.0 and RIN ≥ 7.0 according to the RNA quality assessment. Sequencing and data analysis were performed using the Illumina HiSeq system (Illumina, San Diego, CA, USA). The experimental process was carried out according to the standard procedures provided by Illumina, including the preparation of library and sequencing experiment. After the quality inspection, ribosomal RNA (rRNA) was removed through epicenter ribo zero^{TM}kit produced by the Illumina company. The remaining RNA was purified, recovered and randomly broken into small pieces by fragmentation buffer for RNA library construction. Illumina hiseq4000 was used for RNA sequencing. The reading length is 2 × 150 bp (PF150).

Immunohistochemical staining

Mice tissues were fixed in 10% formalin and embedded in paraffin wax before 4 μL serial sections were cut. The sections were then deparaffinized and rehydrated routinely. The slides were incubated with the following antibodies: anti-α-SMA, anti- Col1a1(CST, MA, USA) for 30 minutes at room temperature, and

maintained overnight at 4°C. Afterwards, the slides were visualized using diaminobenzidine and hematoxylin on the second day.

Actinomycin D and Ranse R treatment assay

Transcription blocking assay was performed through the addition of 2 mg/mL actinomycin D (Med Chem Express, NJ, USA) for 4 h, 8 h, 12 h, and 24 h. To detect the expression level of circ_0008494 and its line isoform ARID1A mRNA, the same amount of RNA was utilized for reverse transcription and quantitative real-time PCR analysis. The RNase R treatment assay was used to verify the stability of circ_0008494. In short, 1 μg of total RNA was incubated with RNase R or DEPC-treated water in 10×reaction system (Epicenter Technologies, Madison, WI, USA) for 30 minutes at room temperature. For the RNase R treatment group, 0.15 μL RNase R （20 U/μL）and 1.5 μL reaction buffer were added. As for the control group, 0.15 μL DEPC-treated water and 1.5 μL reaction buffer were added.

Quantitative real-time PCR (qRT-PCR)

Detection of mRNAs were performed using a qPCR-RT Kit （RR036A, Takara, Tokyo, Japan）and a SYBR Premix Ex TaqTM II Kit （RR820A, Takara, Tokyo, Japan. Detection of circRNAs was performed using Reverse transcription and qRT-PCR kits (R11088.2, Ruibo Bio, Guangzhouou, China). Detection of miRNAs was performed using Reverse transcription and qRT-PCR kits (R10031.7, Ruibo Bio, Guangzhou, China). The primers used for detection of mRNAs and circRNAs are shown in **Table2** and **supplementary Table1**.MiR-185-3p primer, miRNA mimic, miRNA inhibitor and miRNA NC were designed by Ruibo Bio (Guangzhou, China). The mRNA and circRNA levels were normalized to total GAPDH. The miRNA level was normalized to U6.

Western blot analysis

RIPA-PMSF (100:1) buffer (Beyotime, Shanghai, China) was used for cell lysis, and the lysates were separated by SDS-PAGE. Proteins were transferred to polyvinylidene fluoride membranes (Millipore, CA, USA) at 350 mA for 2 h. The membranes were incubated overnight using the primary antibodies at 4° C. After incubation with secondary antibodies (Sigma, CA, USA) for 2 h, the membranes were subjected to chemiluminescence exposure and photographed using a Tannon 3500 imager (Tannon, Shanghai, China). The primary antibodies worked in this paper included anti-α-SMA, Col1a1, FGF5, BRD4 and GAPDH （CST, MA, USA）. The protein levels were normalized to total GAPDH.

Establishment of stable cell line

Three siRNAs targeting the junction site of hsa_circ_0008494 and a negatively controlled siRNA were designed and packaged into a lentiviral vector (No. Gv493, element sequence hu6-mcs-cbh-gcgfp-ires-puromycin). The negatively controlled scramble sequence was TTCTCCGAACGTGTCACGT. LX-2 cells were infected with lentiviral constructs, including LV-circ_0008494-KD1, LV-circ_0008494-KD2, LV-circ_0008494-KD3 and LV-NC. The GFP labeling of the recombinant viruses was confirmed using an inverted fluorescent microscope (Zeiss, Thornwood, USA). The knockdown efficiency of circ_0008494

was confirmed by RT-qPCR assays. To generate a stable circ_0008494-interfering cell line, LX-2 cells infected with LV-circ_0008494-KD3 and LV-NC viruses were selected with 5 μg/mL puromycin. Clones resistant to puromycin were collected and expanded in a culture dish.

miRNA transfection

miRNA products and transfection reagent were purchased from Ruibo Bio (Guangzhou, China). Transfection was carried out according to the manufacturer's instructions. The final transfection concentration was 125nM. For cell function detection or rescue assays, miRNA products were respectively transfected into LX-2 cells, stable LV-circ_0008494-KD LX-2 cells or LV-NC cells. 48 hours after transfection, the cells of each experimental group were re-suspended, collected and subjected to downstream experiments.

CCK-8 assay

LX-2 cells of each experimental group were seeded in 96-well plates overnight at a density of 1×10^3/ mL. After 1, 2, 3, 4 or 5 days, 10 μL CCK-8 (Dojindo, Kumamoto, Japan) was added to each well and incubated for 4 hours at room temperature. The absorbance was measured with a microplate reader at 450 nm.

Trans-well migration assay

LX-2 cells of each experimental group were resuspended and seeded in upper trans-well chambers for the migration assay (Corning, NY, USA) at a density of 1×10^6 cells/mL. The cells were allowed to cross the chamber for 48 hours. The penetrated cells were fixed, stained with 1% crystal violet, and counted under an inverted microscope at a magnification 100× (Zeiss, Thornwood, USA).

Apoptosis analysis

Cell apoptosis was quantified using an Annexin V-APD Single Staining Kit (eBioscience, San Diego, CA, USA). The experimental grouping was carried out as above. Each Falcon tube was added with Annexin V-APC (10 μL) and incubated at 37ºC in the dark for 10~15 minutes. Next, each tube was added with 400 μL 1× Binding Buffer. Apoptosis was detected within 1 hour in a flow cytometer (Beckman Coulter, CA, USA).

Luciferase reporter assay

To detect the binding of hsa_circ_0008494 and miR-185-3p, wild-type of circ_0008494 or its complementary or mutant sequences were inserted into a psiCHECK vector. To detect the binding of Col1a1 and miR-185-3p, the Col1a1 3'UTR and its mutant sequences were inserted into a pMIR vector. Lipofectamine 2000 (Invitrogen, CA, USA) was used to co-transfect the miR-185-3p, which was mimicked with psiCHECK-circ_0008494-WT, psiCHECK-circ_0008494-complementary and psiCHECK-circ_0008494-MUTANT vectors, into 293T cells. Additionally, miR-185-3p inhibitor and inhibitor NC were co-transfected with pMIR-Col1a1-WT 3'UTR and pMIR-Col1a1-MUTANT 3'UTR vectors. 48 hours since the

transfection, the relative luciferase absorbance value of each group was examined with a Dual-Luciferase Reporter Assay System (Promega, Madison, USA) and normalized to Renilla luciferase absorbance values.

AGO-RIP assay

A Simple Chip^{TM} Enzymatic Chromatin IP Kit (CST, MA, USA) was used for RNA immunoprecipitation (RIP) experiments. 1 × 10^7 LX-2 cells were pelleted and re-suspended with an equal pellet volume of RIP Lysis Buffer. The cell lysates (100 μl) were incubated with 5 μg of anti-argonaute-2 (AGO2) antibody (CST, MA, USA) or an isotype-matched IgG (CST, MA, USA) coated beads at 4 ºC overnight, respectively. With the treatment of proteinase K, the immunoprecipitated RNAs were extracted by RNeasy MinElute Cleanup Kit (Qiagen, Hilden, Germany). The abundance of circ_0008494 or miR-185-3p was detected by qRT–PCR assay.

Biotin-coupled miRNA capture

A total of 1 × 10^7LX-2 cells were harvested, lysed and sonicated. The miR-185-3p probe and miRNA NC probe were incubated with the C-1 magnetic beads (Life Technologies, Guilford, CT) at 25 ºC for 2 hours to generate probe-coated beads. The cell lysates were incubated with miR-185-3p probe and miRNA NC probe at 4 ºC overnight. After cleansing with the wash buffer, the RNA complexes bound to the beads were eluted and extracted by RNeasy MinElute Cleanup Kit (Qiagen, Hilden, Germany) for qRT–PCR assay. Biltinylated-miR-185-3p probe was designed and synthesized by Ruibo Bio (Guangzhou, China).

Statistical analysis

Statistical analyses were performed using SPSS software 25.0 and GraphPad Prism 8.0. Statistically significant differences were calculated using Student's *t*-test. Data were expressed as the mean ± SD of three independent experiments and $p<0.05$ was considered to indicate a significant difference. The asterisks *, **and*** stand for $p<0.05$, $p<0.01$and $p<0.001$ respectively.

Results

circRNA expression profiles were screened in human liver fibrosis tissues

The collected liver fibrosis tissues were identified by two pathologists and tissue RNA was extracted for quality control analysis. The chosen tissue samples used for RNA-seq were classified as F1 (two cases), F2 (two cases), F3 (one case) and F4 (one case) through the Metavir semi-quantitative evaluation system (**Table 1**). The results of circRNAs sequencing were analyzed using the Illumina HiSeq system, together with the data of three normal liver tissues searched on NCBI as controls (https://www.ncbi.nlm.nih.gov/Traces/study/?acc=ERP013191, data from the Cambridge Institute University of Cambridge cancer research, UK). Finally, 363 significantly upregulated and 635 significantly downregulated circRNAs were detected in human HF tissues compared to normal liver tissues (**Fig. 1a, b**).

The parental genes of the upregulated circRNAs were analyzed by GO and KEGG enrichment analysis (**Fig. 1c, d**). In GO analysis, the enriched factors were primarily related to aging, cell body fiber, cell activation, or positive regulation of fibroblast proliferation while in KEGG analysis, the enriched factors were mainly related to endocytosis, ECM-receptor interaction, or focal adhesion. The analysis preliminarily indicated that these altered circRNAs might have certain potential functions in the regulation of liver fibrosis.

Hsa_circ_0008494 was upregulated in HF tissues and TGF-β1 activated LX-2 cell

Through clustering heat map and volcano plot analyses, attention was initially drawn to hsa_circ_0008494 with a FC value of 3.40 and pVal(t) of 0.022, which indicated its significant upregulation in RNA-seq samples. Using the circbank database and UCSC Genome Browser**,** hsa_circ_0008494 was found to derive from three exons of the ARID1A (AT-rich interaction domain 1A, located on chromosome 1p36) gene through back-splicing and had a conserved homologous circRNA mmu_circ_0001283 in mouse (http://www.circbank.cn/search.html?selectValue=hsa_circ_0008494). Using the Cy3-labeled-circ_0008494 FISH probe, the location of circ_0008494 was clearly observed and we found circ_0008494 was predominantly localized at the cytoplasm of HSCs in liver fibrotic region (**Fig. 2a**). To confirm the expression of mmu_circ_0001283 in HF, a DMN-induced mouse fibrosis model was successfully established (**Fig. 2b)**. The total RNA of mouse liver tissues was extracted, and qRT-PCR showed that the levels of mmu_circ_0001283 and the liver fibrosis indicators α-SMA and Col1a1 were significantly upregulated in the fibrotic mouse liver tissues, as compared with normal mouse liver tissues (**Fig. 2c**). Furthermore, an addition of 22 human HF tissues were collected and the qRT-PCR showed that circ_0008494 expression increased in HF tissues compared with matched normal liver tissues (**Fig. 2d**).

Hsa_circ_0008494 and another 3 altered ecircRNAs (**Table2**) were selected for further verification in LX-2 cell line. LX-2 cells were stimulated with the fibro-genic factor TGF-β1 (15 ng/ml)[22]. The qRT-PCR results showed that compared with the NC group, the liver fibrosis indicators, α-SMA and Col1a1 were significantly upregulated in TGF-β1 treated group (**Fig. 2e**), indicating that LX-2 cells were successfully activated. Meanwhile, hsa_circ_0008494, hsa_circ_0029332 increased and were consistent with the RNA-seq data. Hsa_circ_0110534 decreased and was consistent with the RNA-seq results. But hsa_circ_0013617 was up-regulated and in contrast to the RNA-seq trend (**Fig. 2e, Table2**). The PCR results were basically in consistent with the sequencing trend, indicating the reliability of RNA-sequencing results. To further confirm the circular characteristics of circ_0008494, actinomycin D (ActD), an inhibitor of transcription, was added in LX-2 cells. As is shown in **Fig. 2f**, circ_0008494 was more stable and resistant to ActD than its line isoform ARID1A mRNA. Moreover, an RNase R digestion assay was performed, and the result further demonstrated that circ_0008494 was resistant to RNase R digestion (**Fig. 2g**).

These results showed that hsa_circ_0008494 or mmu_circ_0001283 was abundantly and conservatively expressed in human or mouse HF tissues. Moreover, hsa_circ_0008494 was located at the cytoplasm of

HSCs and significantly upregulated in the TGF-β1 activated LX-2 cells, indicating that it might play a regulatory role in liver fibrosis as a typical ecircRNA. Thus, circ_0008494 was selected as a promising candidate for further study.

circ_0008494 knockdown inhibited the activation, proliferation, migration of HSCs and promoted their apoptosis

The splice junction of circ_0008494 was verified by Sanger sequencing (**Fig.3a**). Three siRNA interference targets were designed according to circ_0008494 junction sequence information (**Fig. 3a**). Virus packaging were completed and the construction framework of the lentiviral vectors were demonstrated in **supplementary Table2.** LX-2 cells successfully infected with lentiviral constructs LV-circ_0008494-KD1, LV-circ_0008494-KD2, LV-circ_0008494-KD3 and LV-NC were confirmed under a fluorescence microscope (**Fig. 3b**). By qRT-PCR, the KD3 group exhibited the highest reduction in circRNA expression compared with the NC group (**Fig. 3c**). Next, LX-2 cells were infected with the circ_0008494-KD3 or NC lentiviral constructs, and clones resistant to puromycin were collected and cultured. A stable LV-circ_0008494-KD LX-2 cell line and LV-NC cell line were successfully established for subsequent experiments.

The role of circ_0008494 in the development of liver fibrosis was subsequently studied using LV-circ_0008494-KD LX-2 cell line or LV-NC cell line. The liver fibrosis indicators, α-SMA and Col1a1, were detected by qRT-PCR and western blot assays. As is shown in **Fig. 4a, b**, the mRNA and protein expression levels of α-SMA and Col1a1 in circ_0008494-knockdown LX-2 cells significantly decreased. The CCK-8 test showed that the fold change in the OD450 value of the circ_0008494-KD group was lower than that of the NC group from day 2 to 5 (**Fig. 4c**). The trans-well assay showed that the migration ability was also reduced in the circ_0008494-KD group (**Fig. 4d**). Additionally, cell apoptosis test showed that the apoptotic proportion of the circ_0008494-KD group significantly increased than that of the NC group (**Fig. 4e**). These results identified circ_0008494 as a new pro-fibrotic regulator of liver fibrosis, suppressing circ_0008494 inhibited activation, proliferation, migration and promoted the apoptosis of HSCs.

circ_0008494 acted as a sponge of miR-185-3p

miRNAs that can be bound to circ_0008494 were predicted by miRanda and RNAhybrid algorithms, and bioinformatics analysis predicted that miR-185-3p harbored an ideal target site for circ_0008494 (**Fig. 5a**). Five ribonucleotides of miR-185-3p were complementary to 159~163 site of circ_0008494. The entire binding site (GACCA) on circ_0008494 were chemically synthesized and inserted into a psiCHECK vector and named as psiCHECK-circ_0008494-WT. Besides, the binding site was mutated to the complementary mode (CTGGT) and the mutated mode (GCAAG). They were also constructed into the psiCHECK vector and named as psiCHECK-circ_0008494-COMPLEMENTARY or psiCHECK-circ_0008494-MUTANT, respectively (**Fig. 5a**). A luciferase assay was further performed and as is shown in **Fig. 5b**, the luciferase activity was markedly reduced in 293T cells co-transfected with miR-185-3p mimic and circ_0008494-wt plasmid compared with cells co-transfected with circ_0008494-complementary and circ_0008494-mutant plasmids. It was generally known that miRNA function as

components of ribonucleoprotein (RNP) complexes or RNA-induced silencing complexes (RISCs), and AGO2 was one of the most important characterized components of RISCs. An RNA-RIP assay was performed to confirm whether circ_0008494 was associated with miRNA RNP. The results showed that circ_0008494 and miR-185-3p were significantly enriched in AGO2 immunoprecipitated comparing to the control IgG group (**Fig. 5c, d**). Next, a biotin-coupled miRNA capture assay was performed using a biotinylated miR-185-3p probe, followed by RT-qPCR. It was observed a fourfold enrichment of circ_0008494 in the miR-185-3p captured fraction compared with the negative group (**Fig. 5e)**. These results suggested that miR-185-3p was a direct target of circ_0008494 in LX-2 cells. Besides, both of circ_0008494 and miR-185-3p could interact with the AGO2 protein, indicating the possibility of circ_0008494 acting as a miRNA sponge for miR-185-3p.

Suppressing circ_0008494 inhibited activation, proliferation, migration of HSCs and promoted their apoptosis through miR-185-3p

We detected the expression level of miR-185-3p in TGF-β1 stimulated LX-2 cells. The qRT-PCR results showed that miR-185-3p expression in TGF-β1 stimulated LX-2 cells significantly decreased, comparing to the NC group (**supplementary Fig. 2**) in LX-2 cells. Next, LX-2 cells were transfected with miR-185-3p mimic or inhibitor. The qRT-PCR results showed that the mRNA expression levels of α-SMA and Col1a1 significantly decreased in the miR-185-3p mimic transfected group but obviously increased in the miR-185-3p inhibitor transfected group compared with the miRNA NC groups (**Fig. 6a, b)**. Western blot assay demonstrated the same trend, which goes to show that miR-185-3p could well regulate the α-SMA and Col1a1 in protein level (**Fig. 6c)**. In addition, CCK8 and trans-well assays further revealed that miR-185-3p mimic could decrease the proliferation and migration abilities of LX-2 cells, while miR-185-3p inhibitor had an opposite function (**Fig. 6d, e)**. Together, these results suggested that miR-185-3p is an anti-fibrotic regulator in liver fibrosis.

To reaffirm whether the regulatory effect of circ_0008494 on HSCs is dependent on its interaction with miR-185-3p, a rescue assay was designed. miR-185-3p inhibitor was transfected into stable circ_0008494-interfering cell line, while miRNA inhibitor NC was transfected into stable circ_0008494-interfering cell line as a control or into LX-2 NC cells as a normal control. As is shown in **Fig. 7a and b**, the mRNA and protein expression levels of α-SMA and Col1a1 in stable circ_0008494-knockdown LX-2 group transfected by the miRNA inhibitor NC significantly decreased, comparing to the miRNA inhibitor NC transfected LV-NC group, but miR-185-3p inhibitor partially resorted the reduced expression of α-SMA and Col1a1 after it was transfected into the circ_0008494-knockdown LX-2 cells, comparing with the inhibitor NC transfection stable circ_0008494-interfering group. **Fig. 7c, d and e** showed that the proliferation and migration abilities in miRNA inhibitor NC transfected stable circ_0008494-knockdown LX-2 cells were significantly downregulated, but their apoptosis increased in comparison with the miRNA inhibitor NC transfected LV-NC cells. However, miR-185-3p inhibitor is shown to have promoted the proliferation and migration of HSCs and ameliorated their apoptosis after it was transfected into the circ_0008494-knockdown group when compared with the miRNA inhibitor NC transfected stable circ_0008494-

knockdown LX-2 cells. These results suggest that circ_0008494 can regulate the activation and biological function of HSCs by sponging miR-185-3p.

Suppressing circ_0008494 inhibited HSCs activation through the miR-185-3p/Col1a1 axis

Considering that HSCs have a particularly complex regulatory network, we screened target genes of miR-185-3p through literature search and TargetScan website **(Table3)**. The screened candidates FSCN1, MLCK, GREM1, c-Myc, WNT2B, E2F1, BRD4, Col1a1, FGF5, TIMP2 and TGFBR2 were then detected by qRT-PCR in LX-2 cells transfected with miR-185-3p mimic and mimic NC.
As is presented in **supplementary Fig. 3**, Col1a1, FGF5 and BRD4 were significantly downregulated. Among the three genes, Col1a1 showed the most obvious reduction. It was nearly downregulated to 30%, compared to FGF5's 57% and BRD4's 67%. Besides, the three genes were up-regulated in TGF-β1 stimulated LX-2 cells, indicating that they might play a role in HSCs activation (**supplementary Fig. 4**). Western blot analysis confirmed that miR-185-3p mimic down-regulated these gene coding proteins but miR-185-3p inhibitor promoted their expression (**supplementary Fig. 5**). In view of the deposition of collagen 1 playing a key role in the initiation of liver fibrosis, Col1a1 was selected for further research. Using the TargetScan website, we found that seven ribonucleotides of hsa-miR-185-3p were complementary to the 642~648 site of the Col1a1 3'UTR (**Fig. 8a**). The direct binding between miR-185-3p and Col1a1 was validated by dual-Luciferase reporter assay. Compared with cells co-transfected with Col1a1-WT plasmid and miRNA inhibitor NC, the ratio of firefly luciferase to Renilla luciferase was significantly increased in 293T cells co-transfected with Col1a1-WT plasmid and miR-185-3p inhibitor. But there was no significant difference in the ratio of firefly luciferase to Renilla luciferase between Col1a1-MUTANT plasmid and miRNA inhibitor NC group, as compared to Col1a1-MUTANT plasmid and miR-185-3p inhibitor group (**Fig. 8b**). The result confirmed that Col1a1 was, in fact, a target of miR-185-3p.

Col1a1 was a direct target gene of miR-185-3p and Col1a1 itself is also a key indicator of HSCs activation and hepatic fibrosis. To further confirm whether the regulatory effect of circ_0008494 on Col1a1 was dependent on its interaction with miR-185-3p, a rescue assay was designed. miR-185-3p inhibitor or inhibitor NC was transfected into stable circ_0008494-interfering cell line. Quantitative real-time PCR and western blot assays were used to detect the expression of Col1a1. As is shown in **Fig. 8c** and **8d**, miR-185-3p inhibitor significantly reversed the decreased expression of Col1a1 both in mRNA and protein levels in stable circ_0008494-interfering LX-2 cells, whereas inhibitor NC had no effect. Besides, TGF-β1 was used to stimulate the LX-2 cells, mimicking HSCs activation in vivo. After TGF-β1 stimulation, miR-185-3p mimic or miR-185-3p inhibitor was transfected into LX-2 cells, Col1a1 protein decreased in miR-185-3p mimic group but increased in miR-185-3p inhibitor group (**Fig. 8e**). Besides, after TGF-β1 stimulation was run in stable circ_0008494-interfering cells or LV-NC cells, Col1a1 protein increased significantly in LV-NC cells, but showed less remarkable elevation in LV-circ_0008494-KD cells (**Fig. 8f**). Importantly, miR-185-3p inhibitor or inhibitor NC was transfected into the TGF-β1 stimulated LV-circ_0008494-KD cells. MiR-185-3p inhibitor significantly reversed the decreased protein expression of Col1a1 during this stimulation process, whereas inhibitor NC did not have the same effect (**Fig. 8f**). These

results further indicated that circ_0008494 and miR-185-3p could regulate Col1a1 during HSCs activation. Suppressing circ_0008494 inhibited the expression of Col1a1 by freeing of miR-185-3p.

Discussion

Hepatic fibrosis-associated morbidity is progressively increasing worldwide, but successful antifibrotic treatment is still lacking. In addition, uncontrolled HF may eventually progress into irreversible liver injury. HSCs are central players in the pathogenesis of liver fibrosis. Following liver damage, HSCs are activated to produce smooth muscle actin protein and secrete large amounts of ECM[23–25]. Collagens are the most important ECM components in the liver. Suffering from liver injury, the normal matrix of the Disse space is disrupted and replaced by fibrillar collagens, including primarily collagen I and collagen III, especially collagen I. The deposition of type I and type III collagens not only continuously activates HSCs but also keeps them in an active state, thereby causing hepatocyte dysfunction[26]. Thus, inhibition of liver collagen production is critical to the prevention and treatment of HF.

At present, the role of circRNAs as a novel type of competitive endogenous RNA is generally accepted. They contain MREs and can competitively bind to corresponding miRNAs, releasing the downstream target genes from miRNAs. In the past 2 years, circRNAs research in the field of liver fibrosis has received some progress. Some circRNAs, such as circFBXW4, cMTO1 and circ_0004018, have been demonstrated to participate in the regulation of the proliferation and activation of HSCs by sponging miR-18b-3p, miR-181-5p or miR-660-3p and releasing their target genes, including FBXW7, PTEN and TEP1[27–29].

In our research, we were initially concerned about circ_0008494, which is derived from three exons of the ARID1A gene and showed high expression in RNA-seq data. Further experiments confirmed that circ_0008494 and its homologous mmu_circ_0001283 were abundantly and conservatively expressed in human and mouse liver fibrosis tissues. Importantly, FISH assay demonstrated that circ_0008494 was primarily located in the cytoplasm of HSCs of the fibrosis region and circ_0008494 was up-regulated in TGF-β1 activated LX-2 cells. We demonstrated that the activation, proliferation and migration abilities of HSCs were markedly attenuated whereas the apoptotic proportion was significantly increased after circ_0008494 knockdown. These results suggested that circ_0008494 served as a novel pro-fibrotic regulator in the liver fibrosis. We assessed the circ_0008494-associated ceRNA network and miR-185-3p harbored an ideal target site for circ_0008494. Using dual-Luciferase reporter, AGO-RIP and biotin-coupled miRNA capture assays, we confirmed that miR-185-3p was a direct target of circ_0008494.

miR-185-3p has been demonstrated to act as a tumor suppressor in various malignancies, such as nasopharyngeal carcinoma, breast cancer and colorectal cancer[30–32]. In our study, we discovered that miR-185-3p was downregulated in activated HSCs and inhibited the activation of HSCs markedly. Rescue assay demonstrated that suppressing circ_0008494 inhibited the activation, proliferation and migration of HSCs, and promoted their apoptosis through miR-185-3p, at least in part. Quite significantly, we have identified potential downstream targets of miR-185-3p through literature search and bioinformatics analysis. With the help of RT-qPCR and western blot assays, we found that Col1a1, FGF5 and BRD4 were

all possible targets of miR-185-3p in LX-2 cells. Fibroblast growth factors (FGFs) are heparin-binding polypeptides, and function in numerous cellular developmental and metabolic processes. It was reported that FGF5 played significant roles in the pathophysiology of hepatic fibrosis or diet-induced steatohepatitis[33, 34]. BRD4 is a member of the BET family proteins[35]. Huang et al. reported that microRNA-29a could mitigate liver fibrosis in mice by regulating BRD4[36]. However, the deposition of collagen 1 plays a key role in the initiation of liver fibrosis, and among these three genes, Col1a1 showed the most obvious reduction after miR-185-3p mimic transfection in qPCR assay. The luciferase assay further verified that Col1a1 was a direct target gene of miR-185-3p, and rescue assays confirmed that the regulatory effect of circ_0008494 on Col1a1 was dependent on its interaction with miR-185-3p. miR-185-3p inhibitor significantly reversed the lowered levels of Col1a1 in stable circ_0008494-interfering LX-2 cells, both at a normal level and after TGF stimulation. Hence, the circ_0008494/ miR-185-3p/Col1a1 axis was well demonstrated in liver fibrosis.

In conclusion, circ_0008494 was identified as a new pro-fibrotic regulator of hepatic fibrosis. Our study demonstrates that the circ_0008494/miR-185-3p axis not only regulates the proliferation, migration and apoptosis of HSCs, but has the unique ability to regulate the activation of HSCs by directly targeting Col1a1, which is the key indicator of HSCs itself. Knocking down circ_0008494 remarkably ameliorated the expression of Col1a1 by freeing of miR-185-3p. Therefore, the role of circ_0008494/miR-185-3p/Col1a1 axis in HSC activation deserves serious attention, as it may serve as a promising and effective target for the treatment of liver fibrosis.

Interestingly, some other genes were also noted during our study, such as FGF5 and BRD4, which reflects the complexity of the circRNA-miRNA-ceRNA network in HSCs. Our results provide further insight into the ceRNAs network in HF and make a beneficial contribution to the identification of effective therapeutic targets.

Declarations

Acknowledgments:

This work was supported by the National Natural Science Foundation of China (NSFC) with No.81870418,81770600, 81870416, 81800536.

Funding

This work was supported by the National Natural Science Foundation of China (NSFC) with No.81870418,81770600, 81870416, 81800536.

Competing Interests

The authors declare no conflict of interest regarding this study.

Author Contributions

YHY, ZX and LY designed the study. LBB, ZJM, LYY and TKG carried out the experiment in vitro and in vivo. ZLF conducted the animal model. LBB and ZJM analyzed the data and wrote the paper. YHY, ZX and LY revised the manuscript.

Ethical approval

The study was reviewed and approved by the Research Ethics Committee of Second Affiliated Hospital of Naval Medical University, Shanghai, China. Informed written consent was obtained from each sampled patient. The animal experimental methods were approved by the Research Ethics Committee of Second Affiliated Hospital of Naval Medical University, Shanghai, China.

Datasets available

The datasets in this study are available at:

https://www.ncbi.nlm.nih.gov/geo/query/acc.cgi?acc=GSE191247

References

1. Lee YA, Wallace MC, Friedman SL. Pathobiology of liver fibrosis.a translational success story. Gut. 2015;64(5):830.
2. Chien Y, Tsai P, Lai Y, Lu K, Liu C, Lin H, Huang C, Wu W, Wang C. CircularRNA as novel biomarkers in liver diseases. J Chin Med Assoc. 2020;83(1):15–7.
3. Zhang CY, Yuan WG, He P, Lei JH, Wang CX. Liver fibrosis and hepatic stellate cells: Etiology, pathological hallmarks and therapeutic targets. World J Gastroenterol. 2016;22(48):10512–22.
4. Tha B, Slf A, Yh A. Hepatic stellate cells as key target in liver fibrosis - ScienceDirect. Adv Drug Deliv Rev. 2017;121:27–42.
5. Tsuchida T, Friedman SL. Mechanisms of hepatic stellate cell activation. Nat Rev Gastroenterol Hepatol. 2017;14(7):397–411.
6. Ganguly N, Chakrabarti S. Role of long non–coding RNAs and related epigenetic mechanisms in liver fibrosis (Review). Int J Mol Med. 2021;47(3):04856.
7. Ghafouri-Fard S, Abak A, Talebi S, Shoorei H, Branicki W, Taheri M. Akbari Dilmaghani N.Role of miRNA and lncRNAs in organ fibrosis and aging. Biomed Pharmacother. 2021;143:112–32.
8. Yang Y, Lei W, Jiang S, Ding B, Wang C, Chen Y, Shi W, Wu Z, Tian Y. CircRNAs: Decrypting the novel targets of fibrosis and aging. Ageing Res Rev. 2021;70:101390.
9. Song M, Xia L, Sun M, Yang C, Wang F. Circular RNA in Liver: Health and Diseases. Adv Exp Med Biol. 2018;1087:245–57.
10. Jeck WR, Sharpless NE. Detecting and characterizing circular RNAs. Nat Biotechnol. 2014;32(5):453–61.

11. Lasda E, Parker R. Circular RNAs: diversity of form and function. RNA (New York NY). 2014;20(12):1829–42.
12. Jeck W, Sorrentino J, Wang K, Slevin M, Burd C, Liu J, Marzluff W. Sharpless N.Circular RNAs are abundant, conserved, and associated with ALU repeats. RNA (New York NY). 2013;19(2):141–57.
13. Zheng Q, Bao C, Guo W, Li S, Chen J, Chen B, Luo Y, Lyu D, Li Y, Shi G. Circular RNA profiling reveals an abundant circHIPK3 that regulates cell growth by sponging multiple miRNAs. Nat Commun. 2016;7:112–5.
14. Bu F, Zhu Y, Chen X, Wang A, Zhang Y, You H, Yang Y, Yang Y, Huang C, Li J. Circular RNA circPSD3 alleviates hepatic fibrogenesis by regulating the miR-92b-3p/Smad7 axis. Nucleic Acids. 2021;23:847–62.
15. Chen X, Tan Q, Tan X, Li S, Zhang X. Circ_0057558 promotes nonalcoholic fatty liver disease by regulating ROCK1/AMPK signaling through targeting miR-206. Cell Death Dis. 2021;12(9):809.
16. Yang W, Zhao J, Zhao Y, Li W, Zhao L, Ren Y, Ou R, Xu Y. Hsa_circ_0048179 attenuates free fatty acid-induced steatosis via hsa_circ_0048179/miR-188-3p/GPX4 signaling. Aging. 2020;12(23):23996–4008.
17. Jin X, Gao J, Zheng R, Yu M, Ren Y, Yan T, Huang Y, Li Y. Antagonizing circRNA_002581-miR-122-CPEB1 axis alleviates NASH through restoring PTEN-AMPK-mTOR pathway regulated autophagy. Cell Death Dis. 2020;11(2):123.
18. Shen Z, Wu J, Gao Z, Zhang S, Chen J, He J, Guo Y, Deng Q, Xie Y, Liu J, et al. High mobility group AT-hook 1 (HMGA1) is an important positive regulator of hepatitis B virus (HBV) that is reciprocally upregulated by HBV X protein. Nucleic Acids Res. 2022;50(4):2157–71.
19. Han D, Li J, Wang H, Su X, Hou J, Gu Y, Qian C, Lin Y, Liu X, Huang M, et al. Circular RNA circMTO1 acts as the sponge of microRNA-9 to suppress hepatocellular carcinoma progression. Hepatology. 2017;66(4):1151–64.
20. Sunagawa Y, Yamada S, Sonohara F, Kurimoto K, Tanaka N, Suzuki Y, Inokawa Y, Takami H, Hayashi M, Kanda M, et al. Genome-wide identification and characterization of circular RNA in resected hepatocellular carcinoma and background liver tissue. Sci Rep. 2021;11(1):6016.
21. Rattanachaisit P, Suksawatamnuay S, Sriphoosanaphan S, Thanapirom K, Thaimai P, Siripon N, Sittisomwong S, Poovorawan Y, Komolmit P. Stability of hepatitis B virus pregenomic RNA in plasma specimens under various temperatures and storage conditions. PeerJ. 2021;9:e11207.
22. Katsunori Y, Koichi M. Differential Regulation of TGF-β/Smad Signaling in Hepatic Stellate Cells between Acute and Chronic Liver Injuries. Front Physiol. 2012;3:53.
23. Friedman SLHepatic. Stellate Cells: Protean, Multifunctional, and Enigmatic Cells of the Liver. Physiol Rev. 2008;88(1):125–72.
24. Friedman SL. Mechanisms of Hepatic Fibrogenesis. Gastroenterol. 2008;134(6):1655–69.
25. Breitkopf-Heinlein KMC, König C, Gaitantzi H, Addante ATM, Wiercinska E, Cai C, Li Q, Wan F, Hellerbrand C, Hahnel VN. M, et al. BMP-9 interferes with liver regeneration and promotes liver fibrosis. Gut. 2017;66(5):gutjnl–2016.

26. Hernandez-Gea V, Friedman SL. Pathogenesis of Liver Fibrosis. Annu Rev Pathol. 2011;6(1):425–56.
27. Chen X, Li HD, Bu FT, Li XF, Li J. Circular RNA circFBXW4 suppresses hepatic fibrosis via targeting the miR-18b-3p/FBXW7 axis. Theranostics. 2020;10(11):4851–70.
28. Jin H, Li C, Dong P, Huang J, Yu J, Zheng J. Circular RNA cMTO1 Promotes PTEN Expression Through Sponging miR-181b-5p in Liver Fibrosis. Front Cell Dev Biol. 2020;8:714.
29. Li S, Song F, Lei X, Li J, Li F, Tan H. Correction for: hsa_circ_0004018 suppresses the progression of liver fibrosis through regulating the hsa-miR-660-3p/TEP1 axis. Aging. 2021;(12(12)):11517–29.
30. Li G, Wang Y, Liu Y, Su Z, Qiu Y. miR-185-3p regulates nasopharyngeal carcinoma radioresistance by targeting WNT2B in vitro. Cancer Sci. 2015;105(12):1560–8.
31. Lu G, Li Y, Ma Y, Lu J, Chen Y, Jiang Q, Qin Q, Zhao L, Huang Q, Luo Z, et al. Long noncoding RNA LINC00511 contributes to breast cancer tumourigenesis and stemness by inducing the miR-185-3p/E2F1/Nanog axis. J Exp Clin Cancer Res. 2018;37(1):289.
32. Ou C, Sun Z, He X, Li X, Ma J. Targeting YAP1/LINC00152/FSCN1 Signaling Axis Prevents the Progression of Colorectal Cancer. Adv Sci (Weinh). 2020;7(3):1901380.
33. Hanaka H, Hamada T, Ito M, Nakashima H, Tomita K, Seki S, Kobayashi Y, Imaki J. Fibroblast Growth Factor-5 Participates in the Progression of Hepatic Fibrosis. Exp Anim. 2014;63(1):85–92.
34. Nakashima H, Nakashima M, Kinoshita M, Ikarashi M, Miyazaki H, Hanaka H, Imaki J, Seki S. Activation and increase of radio-sensitive CD11b + recruited Kupffer cells/macrophages in diet-induced steatohepatitis in FGF5 deficient mice. Rep. 2016;6:34466.
35. Cai X, Li Z, Zhang Q, Qu Y, Xu M, Wan X, Lu L. CXCL6-EGFR-induced Kupffer cells secrete TGF-β1 promoting hepatic stellate cell activation via the SMAD2/BRD4/C-MYC/EZH2 pathway in liver fibrosis. J Cell Mol Med. 2018;22(10):5050–61.
36. Huang YH, Kuo HC, Yang YL, Wang FS. MicroRNA-29a is a key regulon that regulates BRD4 and mitigates liver fibrosis in mice by inhibiting hepatic stellate cell activation. Int J Med Sci. 2019;16(2):212–20.
37. Ma D, Cao Y, Wang Z, He J, Chen H, Xiong H, Ren L, Shen C, Zhang X, Yan Y. et al.CCAT1 lncRNA Promotes Inflammatory Bowel Disease Malignancy by Destroying Intestinal Barrier via Downregulating miR-185-3p. Inflamm Bowel Dis. 2019;25(5):862–74.
38. Li J, Liu H, Zou L, Ke J, Zhang Y, Zhu Y, Yang Y, Gong Y, Tian J, Zou D, et al. A functional variant in GREM1 confers risk for colorectal cancer by disrupting a hsa-miR-185-3p binding site. Oncotarget. 2017;8(37):61318–26.
39. Liao JM, Lu H. Autoregulatory suppression of c-Myc by miR-185-3p. J Biol Chem. 2011;286(39):33901–9.
40. Gao P, Wang Z, Hu Z, Jiao X, Yao Y. Circular RNA circ_0074027 indicates a poor prognosis for NSCLC patients and modulates cell proliferation, apoptosis, and invasion via miR-185-3p mediated BRD4/MADD activation. J Cell Biochem. 2020;121(3):2632–42.

Tables

Table 1 Clinical data of HF patients for RNA-seq

Gender	Age	Fibrosis stage	HBsAg HBeAg HBcAb	HBsAb HBeAb	ALT (U/L)	AST (U/L)	GGT (U/L)
Female	50	F1	- - +	+ -	17	34	18
Male	53	F1	+ - +	- +	21	13	35
Male	59	F2	- - +	- +	51	44	118
Male	62	F2	+ - +	- +	28	29	21
Male	55	F3	+ + +	- -	69	40	98
Male	56	F4	+ - +	- ±	20	24	93

Note：ALT：Alanine aminotransferase；reference range0~50U/L

AST：aspartate aminotransferase；reference range0~40U/L

GGT：γ-glutamyltransferase；reference range 1~30U/L

Table 2 Information and primer sequences of 4 ecircRNAs

CircRNA	Gene symbol	Position	RNA-Seq	Primer Sequences（5'-3'）
circ_0008494	ARIDIA	chr1:27056141-27059283	Up	**F:** AGATTCATTTGGGTCTCAGGC **R:** ATTGGACTGGATGGAGGCA
circ_0029332	SCARB1	chr12:125279740-125294835	Up	**F:** CTGTCGCAGGCATTGGGTT **R:** GGACTCAGGAGTCATGAAGGG
circ_0110534	HIPK1	chr1:114495387-114500913	Down	**F:** GTCCACCTGCGTTTCAAAAGC **R:** ACAGCCCAGTGACCACATATCAA
circ_0013617	HIPK1	chr1:114483003-114484081	Down	**F:** ACAGTCACGTTACTACAGGTATGGC **R:** CAGTTTCTTCGCACTGCAGAAG

Table 3 Predicted targets of miR-185-3p

Predicted targets	Reported pathways	TargetScan (site type,3`UTR)
FSCN1	LINC00152/miR-185-3p/FSCN1[32]	
MLCK	lncRNA /miR-185-3p/MLCK[37]	
GREM1	miR-185-3p/GREM1[38]	
c-Myc	miR-185-3P/c-Myc[39]	
WNT2B	miR-185-3p/WNT2B[30]	
E2F1	LINC00511/miR-185-3p/E2F1/Nanog [31]	
BRD4	circ_0074027/miR-185-3p/BRD4 /MADD[40]	7mer-m8,642~648
Col1a1		7mer-m8,130~136
FGF5		7mer-A1,596~602
TIMP2		7mer-A1,712~718
TGFBR2		

Figures

Fig. 1

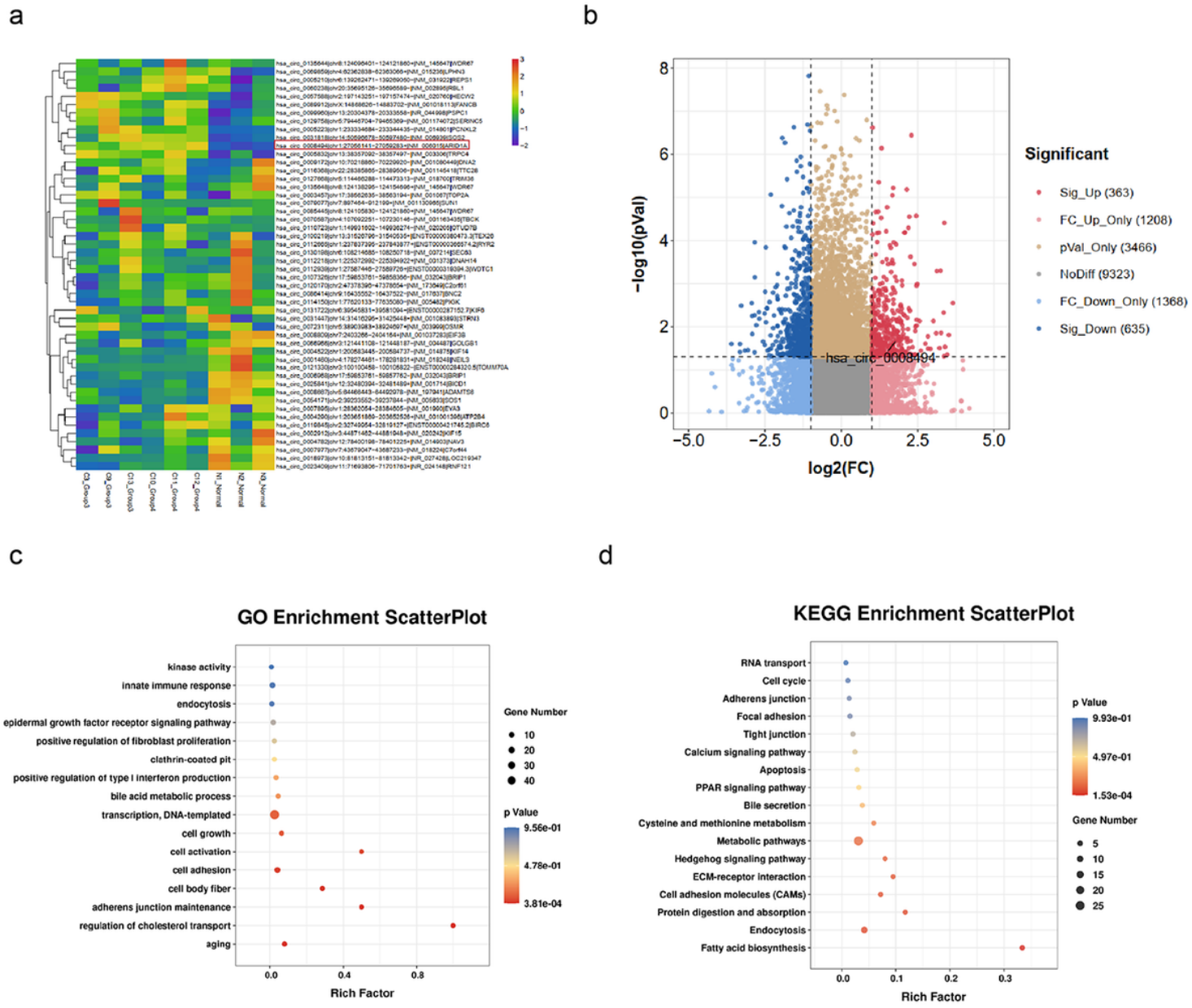

Figure 1

circRNA profiles of human liver fibrosis tissues and circ_0008494 is up-regulated.

a Differential circRNAs clustering heat map. circ_0008494 was up-regulated in HF tissues. Each column represents the expression profile of a HF sample group, and each line corresponds to a circRNA. High expression level is indicated by “red” and lower levels by “blue”.

b Differential circRNAs volcano plot. circ_0008494 was significantly up-regulated. The abscissa is the log2 (Fold Change), and the ordinate is -log10 (p-value). circRNAs with fold changes ≥2 and p-values ≤ 0.05 are indicated as significant up-regulation.

c GO_enrichment_scatterplot of the parental genes of the upregulated circRNAs.

d KEGG_enrichment_scatterplot of the parental genes of the upregulated circRNAs.

Fig. 2

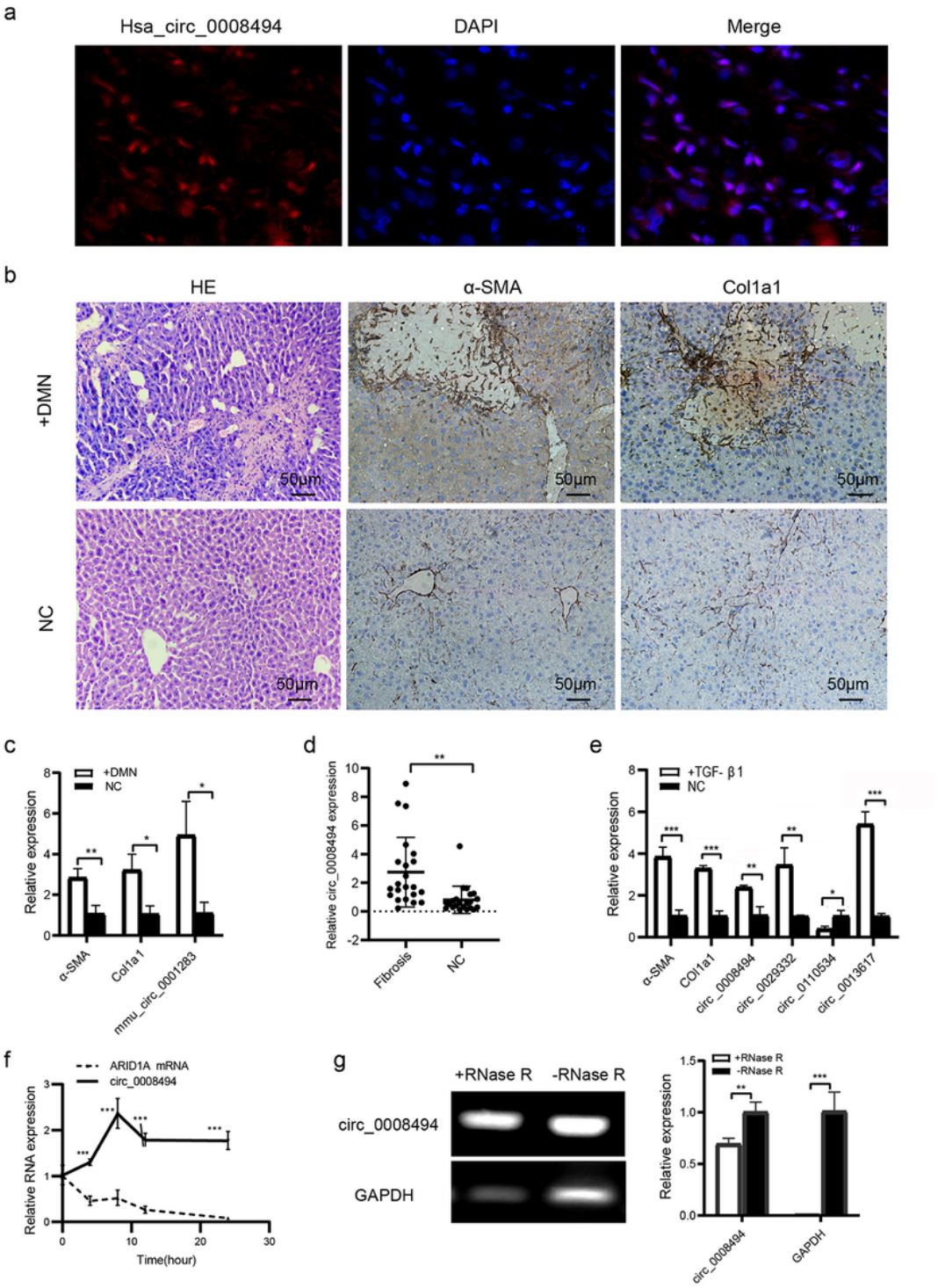

Figure 2

Abundant expression of hsa_circ_0008494 and its homolog mmu_circ_0001283 in HF tissues and HSCs.

a FISH assay revealed that circ_0008494 was predominantly localized at the cytoplasm of HSCs in the fibrotic liver regions. The images were taken under an oil microscope in the area of liver fibrosis. The longitudinal section of HSCs was a long spindle shape, and the transverse section of HSCs was a round or irregular shape(magnification,1000×). Cy3-labeled-circ_0008494 appeared “red”, and nuclei appeared “blue”.

b DMN-induced hepatic fibrotic mice models were established. HE staining showed fatty degeneration, extensive inflammatory cell infiltration and interlobular fibrous septum formation in the DMN-injected group. Immunohistochemistry staining showed obvious expression of α-SMA and Col1a1 in the DMN-injected group(magnification,200×).

c In fibrotic mouse livers, the expression levels of α-SMA, Col1a1 and mmu_circ_0001283 increased, as determined by qRT-PCR assay.

d The expression of circ_0008494 significantly increased in human HF tissues using qRT-PCR assay.

e qRT-PCR assay showed differential expression of circRNAs in TGF-β1 activated LX-2 cells.

f Actinomycin D treatment assay showed circ_0008494 was more stable and resistant to ActD than its line isoform ARID1A mRNA.

g Electrophoresis on agarose gel and qRT-PCR assays showed circ_0008494 exhibited clear resistance to RNase R digestion.

The RNA levels were normalized to total GAPDH. *, ** and ***stand for $p<0.05$, $p<0.01$ and $p<0.001$, respectively.

Fig. 3

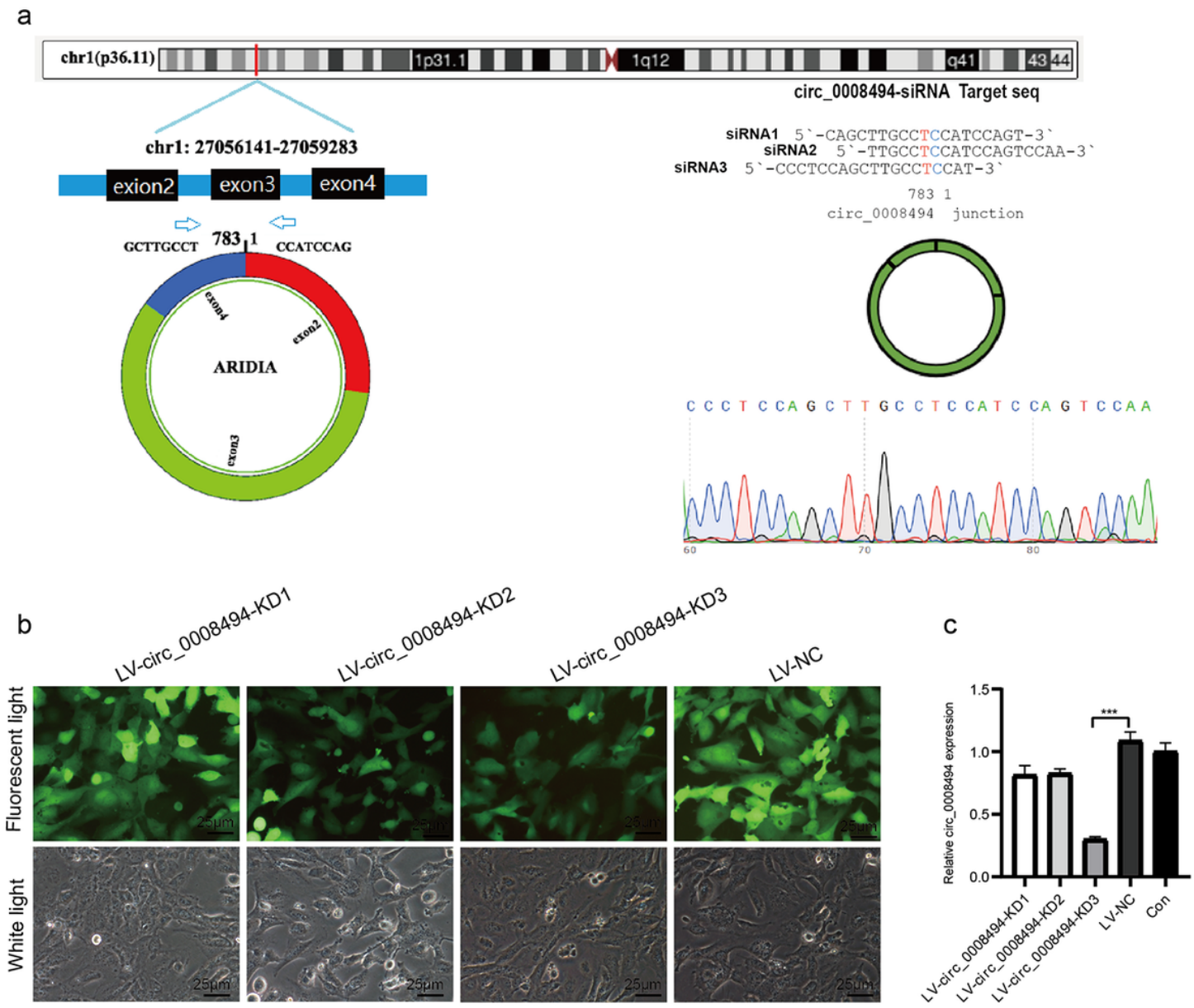

Figure 3

Construction of stable circ_0008494-interfering cell line.

a Structural diagram of hsa_circ_0008494 and construction diagram of hsa_circ_0008494-siRNA target sequences. The splice junction of circ_0008494 was verified by Sanger sequencing.

b LX-2 cells emitted GFP fluorescence after circ_0008494-interfering viruses and NC virus infection (magnification, 400×).

c qRT-PCR was used to detect the expression of circ_0008494 in three different circ_0008494-KD groups and an NC group.LV-circ_0008494-KD3 exhibited the highest reduction (0.30±0.02) vs. LV-NC. The RNA levels were normalized to total GAPDH. *** stand for p<0.001.

Fig. 4

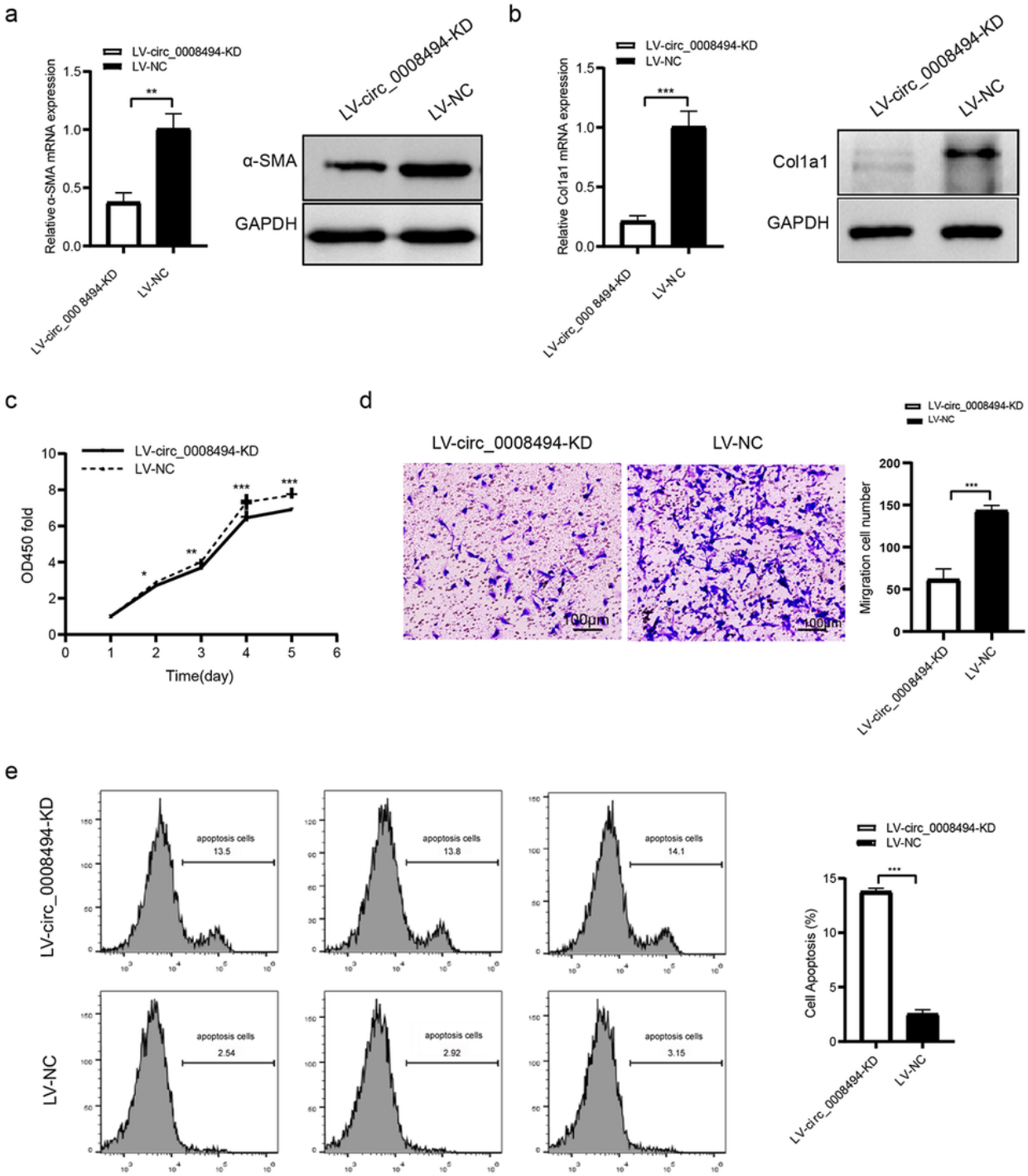

Figure 4

circ_0008494 knockdown inhibits the activation, proliferation, migration of HSCs and promoted their apoptosis.

a The mRNA and protein expression levels of a-SMA in the LV-circ_0008494-KD and LV-NC groups.

b The mRNA and protein expression levels of Col1a1 in the LV-circ_0008494-KD and LV-NC groups.

c Effect of circ_0008494 knockdown on the proliferation of LX-2 cells was detected by CCK8 assay at days 1~5.

d Effect of circ_0008494 knockdown on the migration of LX-2 cells was detected by trans-well assays. The transmembrane cells were photographed and counted at a magnification 100×. Representative pictures are shown.

e Detection of apoptosis by Annexin V-APC single staining combined with flow cytometry in LV-circ_0008494-KD and LV-NC groups. The rate of apoptosis was exhibited in histogram.

The RNA levels were normalized to total GAPDH. The protein levels were normalized to total GAPDH. *, **, and *** stand for $p<0.05$, $p<0.01$ and $p<0.001$, respectively.

Fig. 5

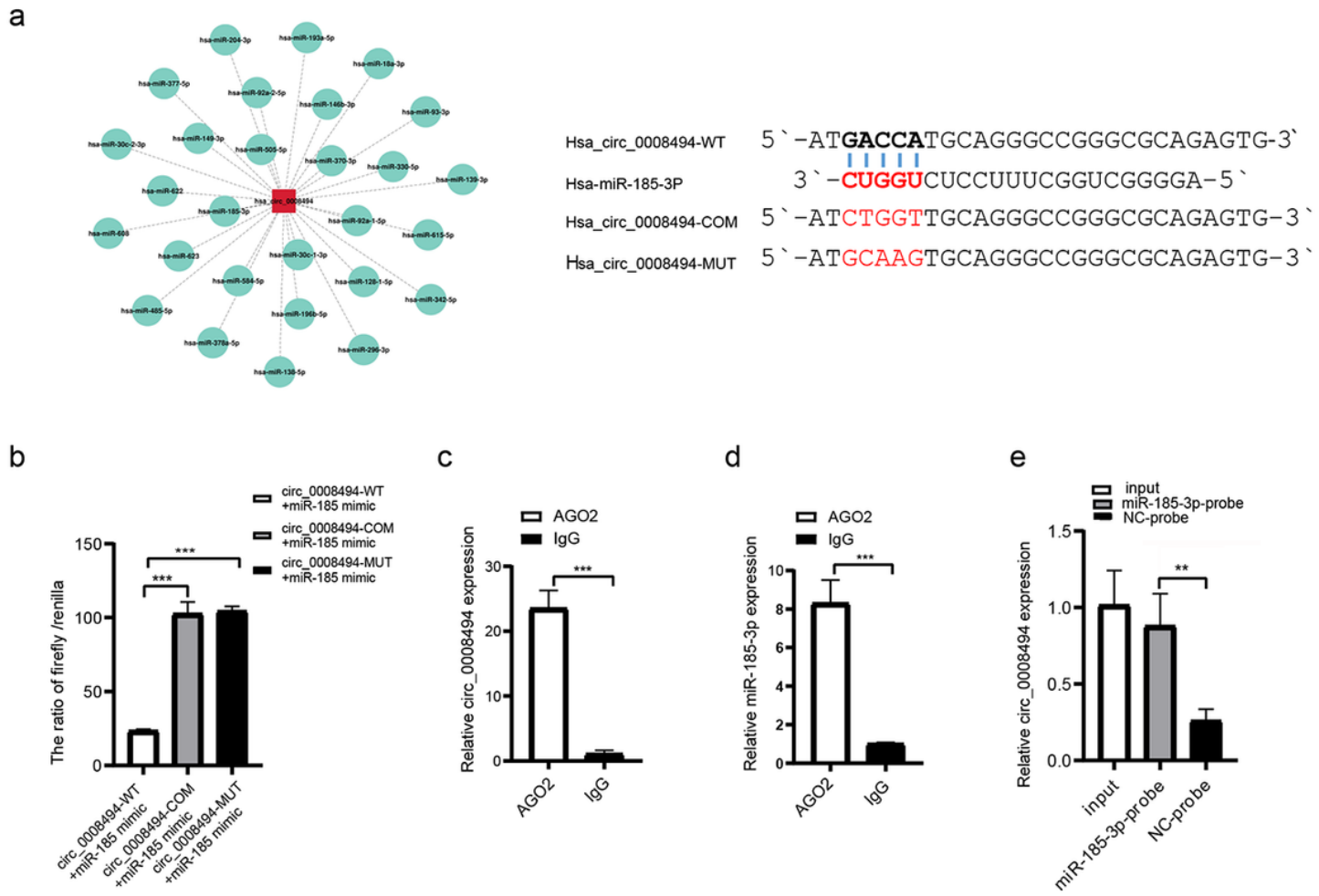

Figure 5

circ_0008494 acts as a sponge of hsa-miR-185-3p

a Bioinformatics prediction of binding sites between circ_0008494 and miR-185-3p.

b Dual-Luciferase reporter gene assay verified the binding relationship between circ_0008494 and miR-185-3p.

c, d Association of circ_0008494 and miR-185-3p with AGO2. Cellular lysates of LX-2 were used for the RIP assay with an AGO2 antibody (IgG as control). circ_0008494 and miR-185-3p levels were detected by qRT-PCR assay.

e Biotin-coupled miRNA capture assay was constructed to verify the binding between circ_0008494 and miR-185-3p using a biotinylated miR-185-3p probe and a miRNA NC probe.

The RNA levels were normalized to total GAPDH. ** and *** stand for $p<0.01$ and $p<0.001$, respectively.

Fig. 6

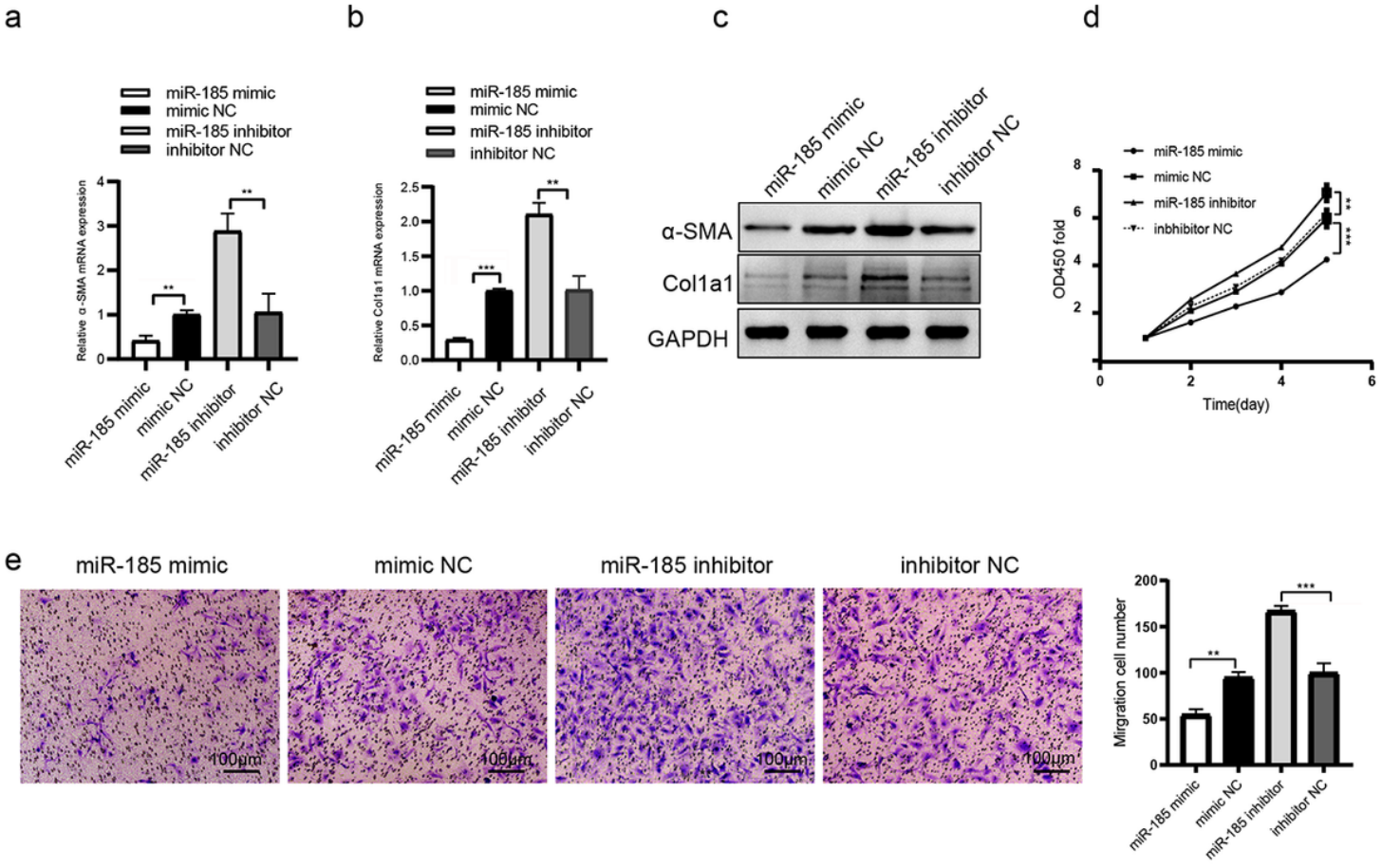

Figure 6

miR-185-3p inhibits HSCs activation, proliferation and migration.

a The mRNA expression of α-SMA was detected by qRT-PCR assay after miR-185-3p inhibitor/mimic transfection.

b The mRNA expression of Col1a1 was detected by qRT-PCR assay after miR-185-3p inhibitor/mimic transfection.

c Western blot assay showed the protein expression of α-SMA and Col1a1 after miR-185-3p mimic or mimic NC transfection.

d Proliferation of LX-2 cells was detected by CCK-8 assay after miR-185-3p inhibitor/mimic transfection at days 1~5.

e Migration of LX-2 cells was detected by trans-well assay after miR-185-3p inhibitor/mimic transfection. The transmembrane cells were photographed and counted at a magnification 100×. Representative pictures are shown.

The RNA levels were normalized to total GAPDH. The protein levels were normalized to total GAPDH. ** and *** stand for $p<0.01$ and $p<0.001$, respectively.

Fig. 7

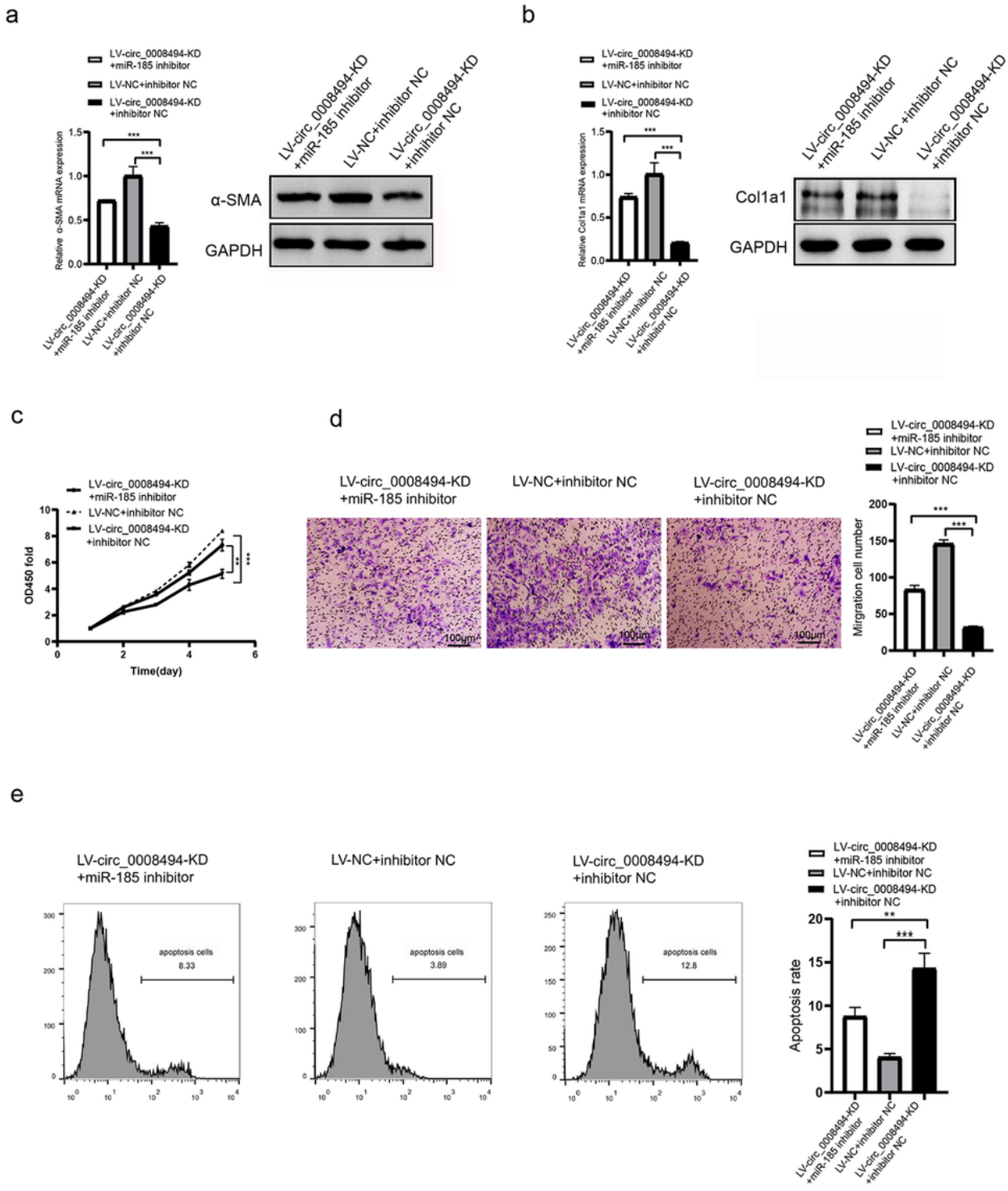

Figure 7

Suppressing circ_0008494 inhibits activation, proliferation, migration of HSCs and promotes their apoptosis through miR-185-3p

a miR-185-3p inhibitor was transfected into stable LV-circ_0008494-KD LX-2 cells. miRNA inhibitor NC was transfected into stable circ_0008494-interfering cell line as a control or LX-2 NC cells as a normal

control. 48 h after transfection, the mRNA and protein expression levels of a-SMA in each group were detected qRT-PCR and western blot assays.

b After transfection as above, the mRNA and protein expression levels of Col1a1 in each group were detected qRT-PCR and western blot assays.

c After transfection as above, proliferation of LX-2 cells in each group was detected by CCK-8 assay

at days 1~5.

d After transfection as mentioned above, trans-well assay showed the migration of cells in each group. The transmembrane cells were photographed and counted at a magnification 100×. Representative pictures are shown.

e After transfection as above, detection of apoptosis by Annexin V-APC single staining combined with flow cytometry was performed in each group. The rate of apoptosis is exhibited in histogram.

The RNA levels were normalized to total GAPDH. The protein levels were normalized to total GAPDH. ** and *** stand for $p<0.01$and $p<0.001$, respectively.

Fig. 8

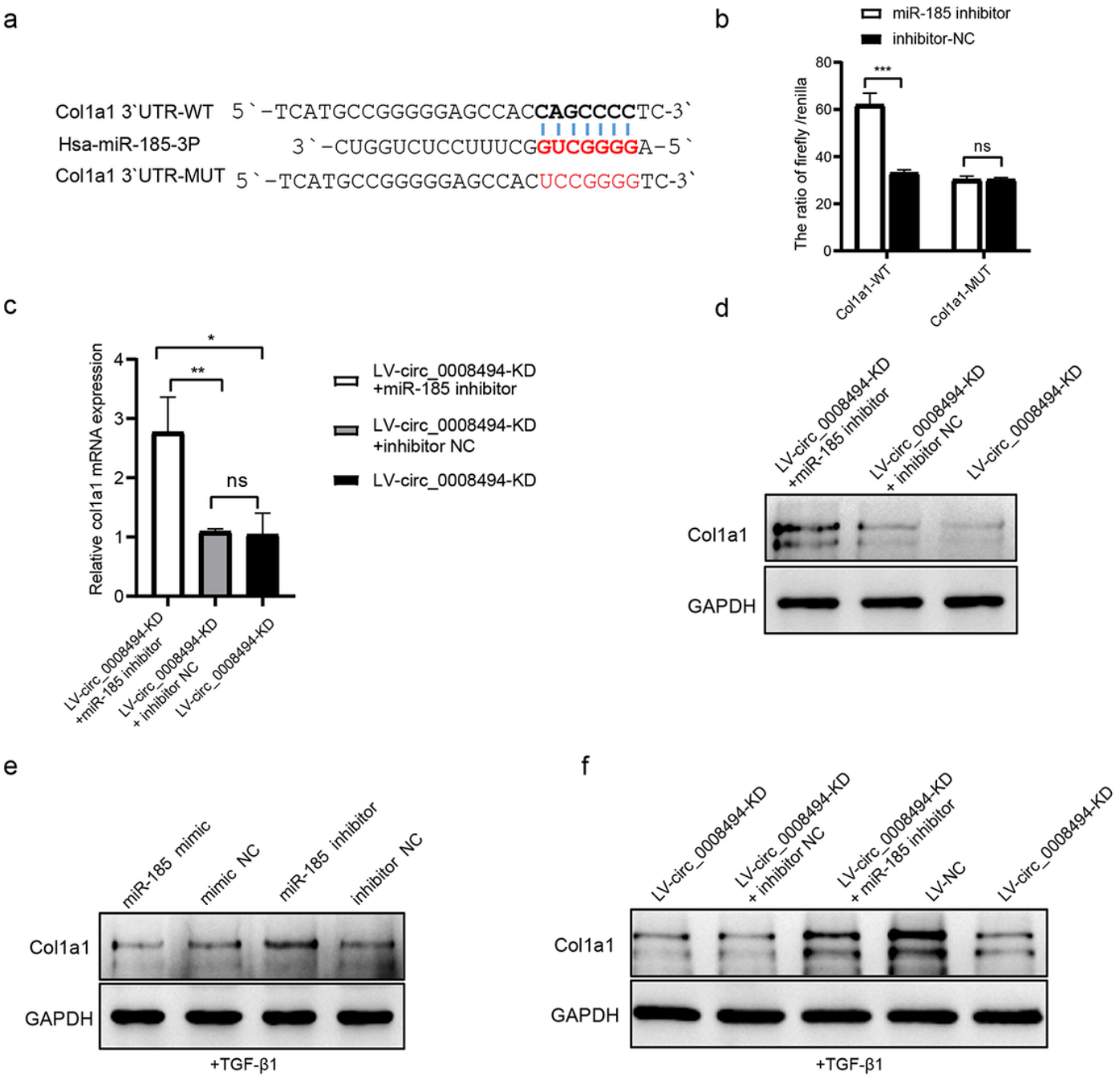

Figure 8

Suppressing circ_0008494 inhibits HSCs activation by regulating the miR-185-3p/Col1a1 axis.

a Bioinformatics analysis technology predicted those seven ribonucleotides of has-miR-185-3p were complementary to the 642-648 sites of Col1a1 3 '- UTR.

b Dual luciferase reporter gene assay verified the binding relationship between miR-185-3p and Col1a1.

c miR-185-3p inhibitor or inhibitor NC was transfected into stable LV-circ_0008494-KD LX-2 cells, and Col1a1 mRNA expression level was detected by qRT-PCR assay.

d miR-185-3p inhibitor or inhibitor NC was transfected into stable LV-circ_0008494-KD LX-2 cells, and Col1a1 protein expression level of was detected by western blot assay.

e After TGF-β1 stimulation, miR-185-3p inhibitor/mimic were transfected into LX-2 cells, and Col1a1 protein expression level were detected by western blot assay.

f After TGF-β1 stimulation of stable LV-circ_0008494-KD cells or LV-NC cells, Col1a1 protein expression was detected by western blot assays. Moreover, miR-185-3p inhibitor or inhibitor NC was transfected into stable LV-circ_0008494-KD LX-2 cells after TGF-β1 stimulation, and Col1a1 protein expression was detected by western blot assays.

The RNA levels were normalized to total GAPDH. The protein levels were normalized to total GAPDH. *, **, and *** stand for $p<0.05$, $p<0.01$ and $p<0.001$, respectively.

Supplementary Files

This is a list of supplementary files associated with this preprint. Click to download.

- 185inhibitor1.jpg
- 185inhibitor2.jpg
- 185inhibitor3.jpg
- 185mimic1.jpg
- 185mimic2.jpg
- 185mimic3.jpg
- 2121146103133RH.jpg
- 2121146103133dpi.jpg
- 2121146103133merge.jpg
- F1100.jpg
- F1200.jpg
- F2100.jpg
- F2200.jpg
- F3100.jpg
- F3200.jpg
- F4100.jpg

- F4200.jpg
- Figure4c6d7cCCK8.xlsx
- Figure1CircRNAExpressionprofile.xlsx
- Figure2Cmmucirc0001283inmouseHFtissue.pzfx
- Figure2Dcirc0008494inhumanHFtissue.pzfx
- Figure2ETFGcircRNA.pzfx
- Figure2FactinomycinD.pzfx
- Figure2GRNase.pzfx
- Figure2c.xlsm
- Figure2dcirc0008494inhumanHFtissue.xlsx
- Figure2e.xlsx
- Figure2fActinomycinD.xlsx
- Figure2gRnaseR.xlsx
- Figure2gRnaseR.scn
- Figure3Cvirus.pzfx
- Figure3acirc0008494andsiRNAdesign.docx
- Figure3asangersequencing.ab1
- Figure3cPCRCircrnaviruspackagingONLX2.xlsm
- Figure4ABLVKD.pzfx
- Figure4CLVcck8.pzfx
- Figure4DTranswell.pzfx
- Figure4EApoptosis.pzfx
- Figure4ab.xlsx
- Figure5B8Bluciferasereporterassays.pzfx
- Figure5Cago2circ0008494.pzfx
- Figure5Dago2miR1853p.pzfx
- Figure5EbiotincoupledmiRNAcaptureassay.pzfx
- Figure5aPredictedmiRNA.xls
- Figure5cdago2.xlsx
- Figure5ebiotincoupledmiRNAcaptureassay.xlsx
- Figure6AB.pzfx
- Figure6Dcck8.pzfx
- Figure6Etranswell.pzfx
- Figure6ab.xlsx

- Figure7AB.pzfx
- Figure7Ccck8.pzfx
- Figure7DTranswell.pzfx
- Figure7Eapoptosis.pzfx
- Figure7ab.xlsx
- Figure8Crescue.pzfx
- Figure8amiR1853pandcol1a1.docx
- Figure8crescueassay.xlsx
- FigureS2185TGF.pzfx
- FigureS2TGFmiR185.xlsx
- FigureS3miR1853ptargetgenes.pzfx
- FigureS3miR1853ptargetgenes.xlsx
- FigureS4TGFCol1a1FGF5andBRD4.pzfx
- FigureS4TGFtargetgenes.xlsx
- HENC200.jpg
- HEDMN200.jpg
- KD1B.jpg
- KD1G.jpg
- KD2B.jpg
- KD2G.jpg
- KD3B.jpg
- KD3G.jpg
- LVKD185inhibitor1.jpg
- LVKD185inhibitor3.jpg
- LVKD185inhibitor1.fcs
- LVKD185inhibitor2.fcs
- LVKD185inhibitor2.jpg
- LVKD185inhibitor3.fcs
- LVKDinhibitorNC1.fcs
- LVKDinhibitorNC1.jpg
- LVKDinhibitorNC2.fcs
- LVKDinhibitorNC2.jpg
- LVKDinhibitorNC3.fcs
- LVKDinhibitorNC3.jpg

- LVKD1.tif
- LVKD2.tif
- LVKD3.tif
- LVNCinhibitorNC1.fcs
- LVNCinhibitorNC1.jpg
- LVNCinhibitorNC2.fcs
- LVNCinhibitorNC2.jpg
- LVNCinhibitorNC3.fcs
- LVNCinhibitorNC3.jpg
- LVNC1.tif
- LVNC2.tif
- LVNC3.tif
- LX2KD1.fcs
- LX2KD2.fcs
- LX2KD3.fcs
- LX2NC1.fcs
- LX2NC2.fcs
- LX2NC3.fcs
- LuciferasereporterassayPlasmidsequence.docx
- Luciferasereporterassayresult.xlsx
- NCB.jpg
- NCG.jpg
- SupplementaryMaterial.docx
- colDMN200.jpg
- colNC200.jpg
- inhibitorNC1.jpg
- inhibitorNC2.jpg
- inhibitorNC3.jpg
- mimicNC1.jpg
- mimicNC2.jpg
- mimicNC3.jpg
- smaDMN200.jpg
- smaNC200.jpg
- wb.pdf